

## Aerosol particles from tropical convective systems: Cloud tops and cirrus anvils

Tomoko Kojima,<sup>1,2</sup> Peter R. Buseck,<sup>1,3</sup> James C. Wilson,<sup>4</sup> J. Michael Reeves,<sup>4</sup>  
and Michael J. Mahoney<sup>5</sup>

Received 31 December 2003; revised 12 April 2004; accepted 5 May 2004; published 25 June 2004.

[1] Aerosol particles from the upper troposphere (UT) and lower stratosphere (LS) were collected during the Cirrus Regional Study of Tropical Anvils and Cirrus Layers-Florida Area Cirrus Experiment (CRYSTAL-FACE) and studied by transmission electron microscopy (TEM). Samples were classified into three categories: (1) UT in-cloud, (2) UT out-of-cloud, and (3) LS. Sulfate particles, including former  $\text{H}_2\text{SO}_4$  droplets, are dominant in samples from all categories. The morphology of  $\text{H}_2\text{SO}_4$  droplets indicates that they had been ammoniated to some extent at the time of collection. They are internally mixed with organic materials, metal sulfates, and solid particles of various compositions. K- and S-bearing organic particles and Si-Al-rich particles are common to the three kinds of samples. In-cloud samples contain abundant Zn-rich particles. Their origin is unclear, but it seems likely that they are contaminants that originated through impact by ice cloud particles on the aircraft or sampling system. Ammoniation and internal mixing of  $\text{H}_2\text{SO}_4$  in the UT aerosols may result in freezing at higher temperature than in pure  $\text{H}_2\text{SO}_4$  aerosols. The relatively high extent of ammoniation in the UT in-cloud samples may have resulted from vertical transport of ammonia by strong convection. Abundances of nonsulfate particles decrease with increasing altitudes. The nonsulfate particles originated from the lower troposphere and were transported to the UT and LS. **INDEX TERMS:** 0305 Atmospheric Composition and Structure: Aerosols and particles (0345, 4801); 0320 Atmospheric Composition and Structure: Cloud physics and chemistry; 0365 Atmospheric Composition and Structure: Troposphere—composition and chemistry; 0368 Atmospheric Composition and Structure: Troposphere—constituent transport and chemistry; **KEYWORDS:** transmission electron microscopy, cirrus clouds, ice nucleation, lower stratosphere, upper troposphere, sulfuric acid

**Citation:** Kojima, T., P. R. Buseck, J. C. Wilson, J. M. Reeves, and M. J. Mahoney (2004), Aerosol particles from tropical convective systems: Cloud tops and cirrus anvils, *J. Geophys. Res.*, 109, D12201, doi:10.1029/2003JD004504.

### 1. Introduction

[2] Tropical cirrus clouds have a large impact on global climate and atmospheric chemistry. The widespread ice clouds reduce incoming solar radiation by scattering sunlight and reduce outgoing infrared energy by absorbing radiation from Earth's surface and lower atmosphere. Thus they affect the radiation budget in the tropics, which, in turn, affects the atmospheric circulation. The net effect on the radiation budget depends on cloud physical properties such as height, thickness, and ice crystal shapes and sizes. Cirrus Regional Study of Tropical Anvils and Cirrus

Layers-Florida Area Cirrus Experiment (CRYSTAL-FACE) was designed to investigate the properties and to better understand cloud formation processes.

[3] In the tropics, cirrus clouds commonly form at the tops of convective clouds (cumulonimbus). Water condenses as liquid cloud droplets in the lower troposphere, is transferred upward through strong convection, and then freezes at sufficiently low temperature to become the ice particles that constitute cirrus clouds. Aerosol particles play important roles in both liquid condensation and freezing, working as cloud condensation nuclei (CCN) and ice nuclei (IN) [Pruppacher and Klett, 1997]. Cirrus clouds also form by slow uplift of air masses, during which water vapor is deposited directly as ice on IN or on ice crystals. Thus the IN could participate by providing a surface that permits ice to be deposited as well as by causing liquid to freeze. During CRYSTAL-FACE, airborne sampling was performed at cloud bases (altitude: 1–3 km), at cloud tops and cirrus anvils (altitude: 12–15 km), and above the tropopause (altitude: 17–18 km). Comparison of particles from different parts of the tropical convective systems could provide insight into the generation and transformation of cloud elements in such systems.

<sup>1</sup>Department of Geological Sciences, Arizona State University, Tempe, Arizona, USA.

<sup>2</sup>Now at Faculty of Science, Kumamoto University, Kumamoto, Japan.

<sup>3</sup>Department of Chemistry and Biochemistry, Arizona State University, Tempe, Arizona, USA.

<sup>4</sup>Department of Engineering, University of Denver, Denver, Colorado, USA.

<sup>5</sup>Jet Propulsion Laboratory, California Institute of Technology, Pasadena, California, USA.

[4] In this paper, we report the results of our transmission electron microscopy (TEM) of aerosol particles collected in the upper troposphere (UT) and lower stratosphere (LS). TEM is uniquely suited for studying relationships between aerosol particles and ice formation because it can provide information about a particle's crystal structure, which is especially important for efficiency as IN [Pruppacher and Klett, 1997]. Previous TEM studies on IN in natural and artificial snow crystals showed that many IN have hexagonal symmetry [Isono, 1955; Kumai, 1961, 1976; Isono *et al.*, 1971] as does ice. A number of TEM studies have been done on UT and LS aerosol particles and have shown that aqueous droplets of  $\text{H}_2\text{SO}_4$  dominate at high altitudes [Bigg *et al.*, 1970; Bigg, 1975, 1980; Ferek *et al.*, 1983; Sheridan *et al.*, 1994]. However, particles collected directly from ice clouds have been less studied using TEM. Chen *et al.* [1998] and Twohy and Gandrud [1998] performed TEM analyses of individual particles collected from cirrus and contrails during Subsonic Assessment: Contrail and Cloud Effects Special Study (SUCCESS) and reported size, composition, and morphology of IN. Our results provide further details on aerosol particles in the tropical UT and LS. Aerosol particles from cloud bases will be considered in a separate paper.

## 2. Sampling and Analytical Method

### 2.1. Sample Collection

[5] Aerosol particles were collected during the July 2002 CRYSTAL-FACE using the Multi-sample Aerosol Collection System (MACS) on the WB-57F aircraft. The MACS uses a thin-plate, low-pressure impactor to collect particles larger than 0.07 and smaller than approximately 3  $\mu\text{m}$  in diameter. Ambient aerosol is sampled from the flow outside the aircraft through a near-isokinetic, passive inlet [Jonsson *et al.*, 1995] and transported to the MACS, which is located inside the aircraft. Particles larger than a few microns in diameter could strike the wall of the sample tube in the 90° bend required to extract the sample flow from the inlet. Upon reaching the MACS, the sample passes through a critical orifice into a plenum to reduce the pressure. Surviving particles larger than a few microns in diameter may also be removed at the front side of this orifice or by collision with the walls of the plenum. A thin-walled impactor plate is positioned over a Cu TEM grid with a Formvar support, and particles are collected on the grid by impaction. The MACS can obtain up to 24 samples per flight. Each sample is on its own TEM grid.

[6] Samples were collected on 26, 28, and 29 July 2002. The MACS started to collect samples shortly after aircraft takeoff and collected samples of 612-s duration with 622-s intervals between samples. Seven to 14 sample grids were obtained on each flight during the 3 days. After each flight the grids were removed from the impactor and stored with desiccants.

[7] The upper size cutoff of the MACS collection system is not precisely known but is expected to be a few micrometers. However, some particles on the grids are larger than a few micrometers, and their presence suggests that other larger particles such as ice crystals may be shattering or bouncing off of surfaces and making it to the TEM grids. We conclude that the samples collected in clouds may

contain some aerosol particles that entered with ice crystals as well as interstitial aerosol.

[8] Simultaneous measurements of particles between 4 and 3000 nm were performed with the Nuclei Mode Aerosol Size Spectrometer (NMASS, particles between 4 and 100 nm) and Focused Cavity Aerosol Spectrometer (FCAS, particles between 80 and 3000 nm). Relative humidity (RH) over ice was determined by measuring the mixing ratio of water and the ambient temperature [May, 1998]. The Harvard Lyman- $\alpha$  water vapor instrument [Weinstock *et al.*, 1994] was also used to obtain RH data.

### 2.2. In-Cloud Versus Out-of-Cloud and UT Versus LS Samples

[9] We determined whether a sample is from clouds on the basis of the data from Cloud, Aerosol, Precipitation Spectrometer (CAPS) [Baumgardner *et al.*, 2001] and the RH over ice. The CAPS was also operated on the WB-57F and measured size distributions of large aerosol and cloud particles. Particles larger than 3  $\mu\text{m}$  in diameter were assumed to be ice, and the cloud-ice-water content was determined from the measured size distributions. We defined samples to be from ice clouds if high ice water content and concentration of large ice particles ( $>3\text{-}\mu\text{m}$  diameter, average  $>0.01\text{ cm}^{-3}$ ) were detected by CAPS and the RH over ice was high (average greater than  $\sim 80\%$ ) during the sampling period. High atmospheric water content for the cloud samples was confirmed by data from the Harvard Lyman- $\alpha$  total water instrument.

[10] The tropopause height was determined by the Microwave Temperature Profiler (MTP) on the WB-57F aircraft [Denning *et al.*, 1989]. The aerosol number concentration and volume concentration, measured by the NMASS and FCAS, respectively, varied over 2.5 orders of magnitude in the UT during the sampling period. This variability extended more than a kilometer above the thermally defined tropopause, whereas measurements of these same properties made more than 1.5 km above the thermal tropopause varied by little more than a factor of 3. The results indicate that the characteristics of UT aerosol do not stop at the measured thermal tropopause but extend some distance above it. We assume that this occurred in the presence of strong convection, either because the measured tropopause is lowered by the convection or because UT aerosols were lofted above the tropopause. Therefore, when we refer to UT aerosols, we include those in the region of high aerosol variability that extends  $\sim 1.5$  km above the measured thermal tropopause.

[11] On the basis of the combined data of the MTP, CAPS, and RH over ice, we categorized nine grids as UT in-cloud samples. CAPS data for grids WB0729#11 and WB0729#12 were not available. The RH over ice for WB0729#12 was above 100%, so this grid is classified as an in-cloud sample. Another 10 are UT out-of cloud samples. Grids WB0728#23 and WB0729#21 sampled some ice particles, but the amounts were minor. We regard four grids collected more than 1.5 km above the tropopause as LS samples. One grid (WB0726#23) was collected when the aircraft was in cloud in the lower troposphere (LT) (altitude: 5–6 km). The CAPS did not detect much ice in the clouds. Table 1 summarizes the sampling conditions for these grids together with data from the NMASS and CAPS.

**Table 1.** Sampling Conditions for Analyzed Grids<sup>a</sup>

Sample	Date, UT	Time, UT		Altitude, <sup>b</sup> km	RH Over Ice, %	NMASS, <sup>c</sup> # cm <sup>-3</sup>	CAPS <sup>d</sup>	
		Start	End				Xtal Conc., # cm <sup>-3</sup>	IWC, g m <sup>-3</sup>
UT In-Cloud Samples								
WB0726#18	26 July	1904	1915	13–16	96	63.2	0.026	2.8 × 10 <sup>-4</sup>
WB0728#17	28 July	2055	2105	14–15	84	54.1	0.53	8.3 × 10 <sup>-3</sup>
WB0728#18	28 July	2115	2126	14	78	62.8	0.47	9.2 × 10 <sup>-3</sup>
WB0728#19	28 July	2136	2146	14–15	103	57.1	3.4	1.5 × 10 <sup>-1</sup>
WB0728#20	28 July	2157	2207	14	82	57.6	0.86	2.4 × 10 <sup>-2</sup>
WB0728#22	28 July	2238	2248	13–15	110	47.2	1.6	2.7 × 10 <sup>-2</sup>
WB0729#12	29 July	1547	1557	13	107	29.8	n. m.	n. m.
WB0729#22	29 July	1913	1923	13–14	80	34.1	1.9	2.9 × 10 <sup>-2</sup>
WB0729#23	29 July	1933	1944	13	89	26.4	0.54	4.6 × 10 <sup>-3</sup>
UT Out-of-Cloud Samples								
WB0728#15	28 July	2014	2024	16	23	46.2	n. d.	2.7 × 10 <sup>-9</sup>
WB0728#16	28 July	2034	2044	14–16	33	52.0	n. d.	1.1 × 10 <sup>-8</sup>
WB0728#23	28 July	2258	2308	16	20	68.6	0.007	2.8 × 10 <sup>-6</sup>
WB0729#11	29 July	1527	1537	13–14	52	50.5	n. m.	n. m.
WB0729#14	29 July	1628	1638	13	61	49.0	1.0 × 10 <sup>-5</sup>	1.6 × 10 <sup>-8</sup>
WB0729#17	29 July	1730	1740	17	22	72.8	n. d.	3.8 × 10 <sup>-9</sup>
WB0729#18	29 July	1751	1801	15–17	14	65.3	n. d.	4.7 × 10 <sup>-9</sup>
WB0729#19	29 July	1811	1821	14–15	41	43.9	n. d.	8.7 × 10 <sup>-9</sup>
WB0729#20	29 July	1832	1842	14	54	33.0	n. d.	2.1 × 10 <sup>-8</sup>
WB0729#21	29 July	1852	1902	14	17	36.9	0.008	4.6 × 10 <sup>-9</sup>
LS Samples								
WB0726#17	26 July	1844	1854	17–18	27	76.6	n. d.	1.9 × 10 <sup>-9</sup>
WB0728#12	28 July	1912	19:22	18	12	67.5	n. d.	2.4 × 10 <sup>-9</sup>
WB0728#14	28 July	1953	2003	18	10	52.7	n. d.	1.9 × 10 <sup>-9</sup>
WB0729#16	29 July	1709	1720	18	16	72.2	n. d.	1.4 × 10 <sup>-9</sup>
LT Sample								
WB0726#23	26 July	2047	2058	5–7	0.3	35.9	2.7 × 10 <sup>-4</sup>	9.5 × 10 <sup>-8</sup>

<sup>a</sup>Here, n. m., not measured; n. d., not detected.<sup>b</sup>Geometric/GPS altitude.<sup>c</sup>Concentration of aerosol particles between 50 and 100 nm diameter (Ch 5).<sup>d</sup>Xtal conc., concentration of crystalline particles larger than 3  $\mu\text{m}$  across; IWC, ice water content.

[12] Particle number concentrations measured by NMASS and FCAS are independent of crystal concentrations for concentrations below  $1 \text{ cm}^{-3}$ , suggesting that they represent the interstitial aerosol particles except in the densest clouds sampled. It seems that the in-cloud samples collected by the MACS consist largely of interstitial particles with some particles associated with ice crystals.

### 2.3. Analytical Method

[13] Aerosol particles were analyzed using a JEOL 2000FX transmission electron microscope operated at 200 kV. Particles were located at low magnification (5000–10,000X) and relatively low electron current density ( $<30 \text{ pA cm}^{-2}$ ) in order to reduce radiation damage. A KEVEX energy-dispersive X-ray spectrometer (EDS) attached to the microscope provided qualitative compositions of individual particles. The EDS system can detect elements with  $Z > 4$ . Structural information was obtained using selected-area electron diffraction (SAED).

[14] Many particles have low contrast and are beam-sensitive, volatilizing through electron radiation. Their EDS spectra show significant peaks for S and O. SAED patterns from similar but larger particles matched those for  $(\text{NH}_4)_2\text{SO}_4$  (mascagnite). We regard the volatile, S- and O-rich particles as ammonium sulfate, although some may also be the bisulfate. Many show a characteristic morphology consisting of a main central particle surrounded by a ring of numerous tiny satellite particles (Figure 1a). Accord-

ing to previous TEM studies, such groups of particles represent former droplets of aqueous  $\text{H}_2\text{SO}_4$  in the atmosphere [Bigg, 1975, 1980; Gras and Ayers, 1979; Ferek et al., 1983; Sheridan et al., 1994]. Droplets originally impacted as  $\text{H}_2\text{SO}_4$  may react with ammonia and partly convert to ammonium sulfate after collection, but they would retain their characteristic morphology. We use the term “ $\text{H}_2\text{SO}_4$  droplet” for the group of these clustered ammonium sulfate particles for the sake of convenience, although they are no longer aqueous.

[15] Most particles can be grouped into one of the following categories (Figure 1): (1)  $\text{H}_2\text{SO}_4$  droplets, (2) ammonium sulfate particles, (3) organic particles, (4) Si-Al-rich particles, and (5) Zn-rich particles. Details of each category are given below.

[16] Particle size distributions were determined from TEM images. Three to five images per grid were taken at magnifications of 1000–5000X from areas approximately  $70 \mu\text{m}$  from the impaction center so that we could see many particles and yet avoid areas where they are superimposed. The longest dimension of each particle larger than  $0.05 \mu\text{m}$  was manually measured on the images. For  $\text{H}_2\text{SO}_4$  droplets we measured the diameters of core particles and rings of satellite particles. Following initial EDS and SAED measurements several types of particles could be identified from their morphology and contrast in the TEM images. For those particles that were difficult to classify in this way, we reinserted the grid into the microscope, located the particle,

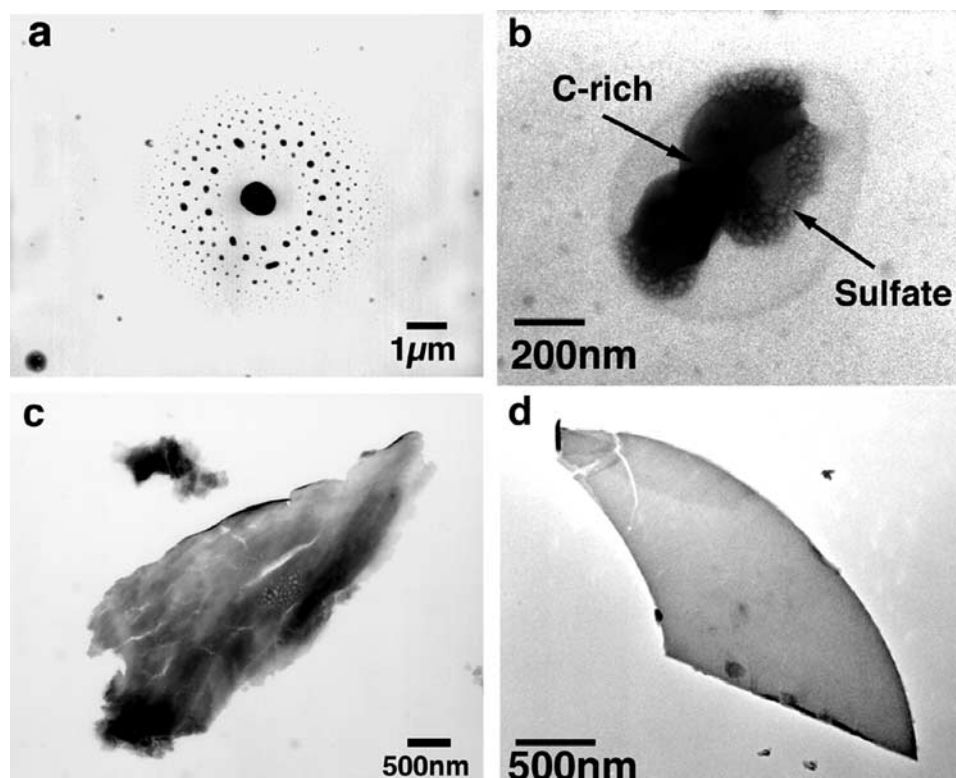


**Figure 1.** Major types of particles in the UT and LS samples. (a)  $\text{H}_2\text{SO}_4$  droplet (center) and presumed ammonium sulfate particles, (b) organic particle, (c) Si-Al-rich particles, and (d) Zn-rich particle. The organic particle (C-rich) is aggregated with sulfate and surrounded by a round rim (cloudy area in Figure 1b).

and obtained EDS data to check the identity. We counted and measured between 120 and 500 particles per grid, with the number depending on particle loading (Table 2), and obtained particle size distributions and aerosol compositions.

[17] Distributions of particles on the grids are not uniform, with more and larger particles occurring near the impaction centers. Because we used images obtained from such areas, the particle size distributions determined by the above procedure are likely biased toward larger particles than the original samples. Also, the aerosol compositions may overestimate particles that have relatively large sizes. However, we used the same procedure for all samples, and therefore compositions among samples are internally consistent.

### 3. Results

#### 3.1. Major Types of Aerosol Particles

##### 3.1.1. $\text{H}_2\text{SO}_4$ Droplets

[18] All  $\text{H}_2\text{SO}_4$  droplets (Figure 1a) in our samples contain central particles of ammonium sulfate, which suggests that they were partially ammoniated prior to collection [Bigg, 1975, 1980; Ferek *et al.*, 1983; Sheridan *et al.*, 1994]. The previous studies proposed that the size of the central particle relative to the size of the whole droplet increases with extent of ammoniation. Several models exist for determining the original sizes of airborne  $\text{H}_2\text{SO}_4$  droplets from TEM images, and the calculated sizes vary considerably depending on which model is used [Gras and Ayers, 1979]. In any case, we believe that the ratio of the diameters of the central particle to the satellite ring

should be a good indicator of the extent of ammoniation in comparing samples. The ratios for the three kinds of samples are shown in Figure 2.

[19] Many particles leave residues after the ammonium sulfate in them volatilizes through electron radiation (Figures 3a and 3b). EDS analysis indicates that the residues consist mainly of C and S. They are probably organic

**Table 2.** Relative Abundances of Particle Types

Sample	$N^a$	Aerosol Composition <sup>b</sup>					
		H <sub>2</sub> SO <sub>4</sub>	AS <sup>c</sup>	Organic	Si-Al	Zn-Rich	Other
<i>UT In-Cloud Samples</i>							
WB0726#18	172	13.95	73.84	4.07	0.58	6.98	0.58
WB0728#18	217	7.37	82.03	0.92	0.92	8.76	0.00
WB0728#19	484	25.62	34.50	0.41	1.65	37.81	0.62
WB0728#22	312	19.87	34.29	2.24	2.56	41.03	0.00
WB0729#22	146	6.16	54.11	2.74	7.53	28.77	0.68
<i>UT Out-of-Cloud Samples</i>							
WB0728#15	371	27.76	65.77	0.54	4.04	1.35	0.54
WB0728#16	490	32.24	66.53	0.61	0.20	0.00	0.41
WB0728#23	124	40.32	52.42	0.81	5.65	0.81	0.00
WB0729#14	312	33.01	43.59	19.55	3.21	0.32	0.32
WB0729#21	150	38.67	52.00	4.67	3.33	1.33	0.00
<i>LS Samples</i>							
WB0728#12	162	33.95	63.58	0.62	1.23	0.00	0.62
WB0728#14	252	10.32	88.49	0.40	0.79	0.00	0.00
WB0729#16	268	27.99	70.52	0.00	1.49	0.00	0.37

<sup>a</sup>Number of counted particles.

<sup>b</sup>Percentage by number.

<sup>c</sup>Ammonium sulfate.

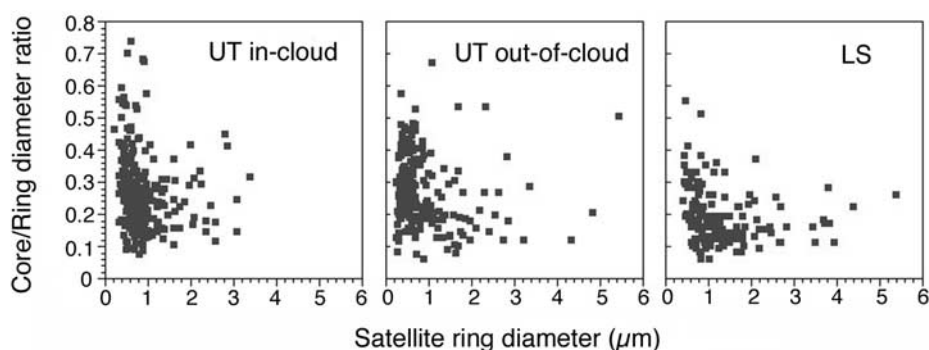


**Figure 2.** Size versus core/rim ratios of  $\text{H}_2\text{SO}_4$  droplets in UT in-cloud samples, UT out-of-cloud samples, and LS samples.

materials that were internally mixed with  $\text{H}_2\text{SO}_4$ . Similar organic residues were reported from ammonium sulfate particles in the boundary layer [Buseck and Pósfai, 1999; Pósfai and Molnár, 2000; Li et al., 2003a, 2003b]. Some residues also contain significant amounts of Mg, Ca, K, and Fe. Their compositions suggest that sulfates or hydroxides of these metals were mixed with  $\text{H}_2\text{SO}_4$ . One to several tiny particles  $\sim 50$  nm in diameter occur in some residues (Figure 3c). They are rich in either transition metals (Fe, Cr, Ti, Zn), C, or Si and Al.

### 3.1.2. Ammonium Sulfate Particles

[20] Many tiny round particles (50–300 nm across) occur in all samples (Figure 1a). They immediately volatilize when exposed to electron radiation, so it is difficult to obtain compositional and structural information for them. Most such particles show similar contrast on TEM images to those of particles in the satellite rings of the  $\text{H}_2\text{SO}_4$  droplets, and their rate of evaporation by electron radiation is similar to that of the satellite particles. EDS spectra from relatively large ones show a small S peak. From these observations we believe that the particles are ammonium sulfate or bisulfate. It is not certain whether they were ammoniated prior to or after collection.

### 3.1.3. Organic Particles

[21] These are single particles or aggregates of two or three spherical to spheroidal C-rich units (150–300 nm across) (Figure 1b). They have relatively uniform sizes (Figure 4) and are distinct from soot aggregates in that (1) aggregation of more than four units is rare, (2) the individual units are larger than 100 nm, and (3) they are amorphous (no spots or rings on SAED patterns) and do not show graphitic layers like soot spherules do at high magnification [Pósfai et al., 1999, 2003; Popovitcheva et al., 2000; Li et al., 2003b]. Besides C, the particles contain significant amounts of N, O, K, and S. They are commonly aggregated with ammonium sulfate (Figure 1b). Many are surrounded by rims with round outlines (Figure 1b).

### 3.1.4. Si-Al-Rich Particles

[22] All samples contain particles rich in Si, Al, and O with minor Fe. The composition suggests that these particles are of crustal origin. However, they differ from soil particles collected from the cloud bases in some respects and are thus treated separately from clay particles (e.g., section 3.1.6). The Si-Al-rich particles do not contain other elements common in crustal particles (K, Mg, Ca, etc.), and the Si/Al ratio varies from one particle to another. SAED patterns

show subtle, diffuse rings, indicating that they are poorly crystalline. Most particles (20 nm to  $>3$   $\mu\text{m}$  across) have flaky appearances with irregular outlines (Figure 1c). Some have rod-like shapes and form clusters of a few microns in diameter. Many have thin coatings of volatile S-rich material, probably ammonium sulfate.

[23] The Si-Al-rich particles are especially abundant in sample WB0726#23, which was collected in clouds in the LT (Table 1).

### 3.1.5. Zn-Rich Particles

[24] Particles of this type are abundant in the UT in-cloud samples. They have angular to irregular shapes, appearing to be thin plates of uniform thickness or crumpled films (Figures 1d and 5). They range from 50 nm to a few micrometers across. Their amounts and size distributions vary among samples, apparently related to the volumes of ice crystals detected during the sampling periods; that is, samples collected when there were large volumes of ice crystals contain more and larger Zn-rich particles (Tables 1 and 2). EDS analysis shows that they are rich in Zn. Most particles also contain O, and many show minor spectral peaks of one or more of C, N, Al, Ni, Fe, Cu, Ti, Cr, Sn, and Pb. Many of these particles have coatings that are typically rich in Zn and S (Figure 5b). C, K, Ca, Fe, Na, and Cl are also common components of the coatings.

[25] The angular to irregularly shaped Zn-rich particles are commonly associated with relatively large ( $>300$  nm) round particles rich in S (Figures 3b and 5a) that also contain significant amounts of Zn and are similar in composition to the coatings of the Zn-rich particles mentioned above. The composition and appearance in TEM images suggest that these round particles were droplets containing dissolved Zn sulfate.

### 3.1.6. Other Kinds of Particles

[26] Several samples contain clay particles. They are in irregularly shaped plates up to 300 nm across. SAED patterns show distinct, hexagonally arranged spots. On the basis of their SAED patterns and compositions the particles were identified as illite and montmorillonite.

[27] Minor amounts of soot aggregates occur in many samples. They show the typical chain-like morphology [Katrinak et al., 1992; Pósfai et al., 1999, 2003; Li et al., 2003b] and range from 100 nm to a few micrometers across. Some are aggregated with ammonium sulfate or organic materials.

[28] A few grains (2–3  $\mu\text{m}$  across) of metallic Al and  $\text{Al}_2\text{O}_3$  were found. The metallic Al is rich in Cr. Fe-oxide particles (1–1.5  $\mu\text{m}$  across) were in two UT in-cloud samples.

### 3.2. UT In-Cloud Samples

[29] All samples contain significant amounts of Zn-rich particles as well as  $\text{H}_2\text{SO}_4$  droplets and ammonium

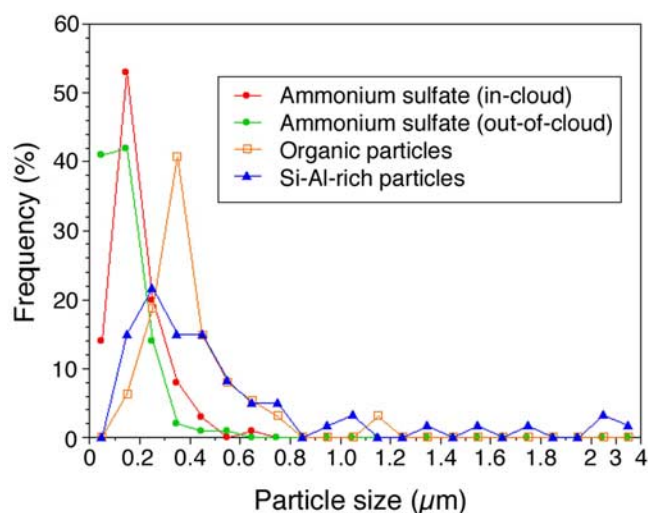
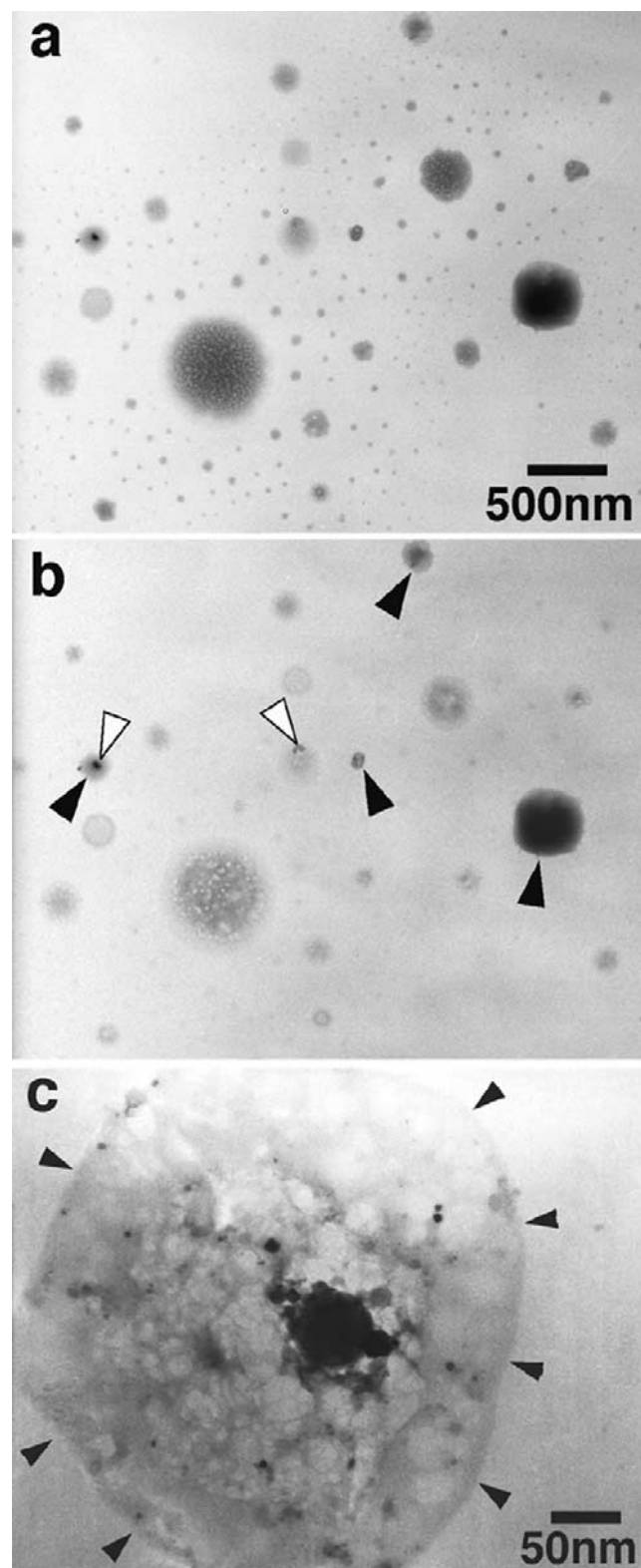


**Figure 4.** Size distributions of ammonium sulfate, organic, and Si-Al-rich particles.

sulfate particles (Table 2 and Figure 5). Round particles of Zn sulfate are also abundant and increase in number with increasing Zn-rich particles and thus with the amounts of ice particles during the sampling period (Figures 3b and 5a). Some are mixed with ammonium sulfate and bubble in the electron beam. Ammonium sulfate particles mixed with Zn sulfate have larger sizes than pure ammonium sulfate particles in the out-of-cloud samples (Figure 4).

[30] The  $\text{H}_2\text{SO}_4$  droplets are relatively small (mostly  $<1$   $\mu\text{m}$  across, Figure 2). The ratio of the central particle diameter to the satellite ring diameter has a wide range (Figure 2), and there is no clear correlation between the ratio and size of the  $\text{H}_2\text{SO}_4$  droplet.

[31] Si-Al-rich particles occur as both large ( $\sim 5$   $\mu\text{m}$ ) single particles and clusters of smaller ones (300 nm). Most organic particles are aggregated with ammonium sulfate and surrounded by round rims.

### 3.3. UT Out-of-Cloud Samples

[32]  $\text{H}_2\text{SO}_4$  droplets and ammonium sulfate particles comprise more than 75% of all particles (Table 2 and Figure 6). Many ammonium sulfate particles larger than 3  $\mu\text{m}$  across occur at the impaction center (Figure 7a). Because they occur where particle loading is extremely heavy and particles are superimposed on one another, it is not clear whether these large particles have satellite

**Figure 3.**  $\text{H}_2\text{SO}_4$  droplets and ammonium sulfate particles from an in-cloud sample (a) before and (b) after intense radiation in the TEM.  $\text{H}_2\text{SO}_4$  droplets (those with satellite textures in Figure 3a) have much weaker contrast in Figure 3b than in Figure 3a. Cloudy residues rich in C and S remain in Figure 3b. Some residues contain tiny solid particles (indicated by white arrows). Most particles that did not change their contrast (indicated by black arrows in Figure 3b) are Zn sulfate. (c) Residue from central particle in a  $\text{H}_2\text{SO}_4$  droplet. Its outline is indicated by arrows. Fe-Cr-oxide particles are in the center of the residue.

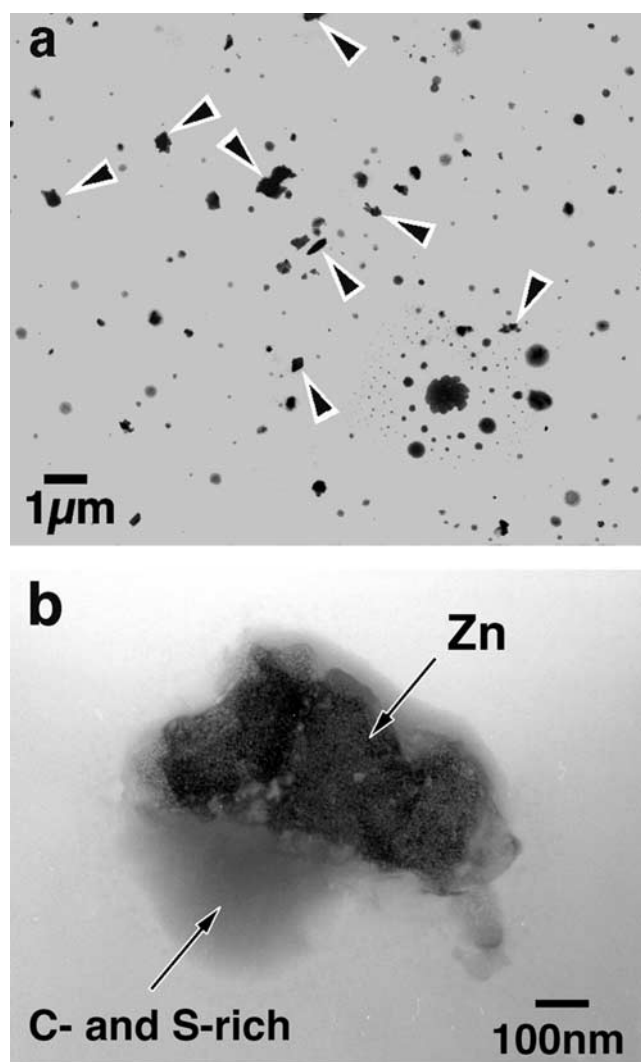


**Figure 5.** (a) Low-magnification image of an area in a UT in-cloud sample. Most angular and irregularly shaped particles with dark contrast are rich in Zn (some are indicated by arrows). Round sulfate particles rich in Zn are also abundant. A  $\text{H}_2\text{SO}_4$  droplet is in the lower right. (b) A Zn-rich particle with a C- and S-rich coating.

textures, and the large sulfate particles are not included in the size analysis shown in Figure 2. Most have circular to irregularly shaped rims (Figure 7a). The rims resemble those that form when aqueous droplets impact onto carbon-coated TEM grids (Figure 1 of *Levin et al.* [1990]). The occurrence of the rims suggests that the sulfate particles originally contained considerable water. Some enclose one or more organic or Si-Al-rich particles. There is an apparent tendency for the  $\text{H}_2\text{SO}_4$  droplets to be less ammoniated than those in the in-cloud samples (Figure 2).

[33] In contrast to the in-cloud samples, Zn-rich particles are rare. They are small ( $<80$  nm) and mainly occur in the center particles of  $\text{H}_2\text{SO}_4$  droplets. Zn-sulfate particles are also rare. On the other hand, Si-Al-rich and organic particles are abundant (Figure 6). Some Si-Al-rich particles are large ( $>3$   $\mu\text{m}$ ). Many organic particles are aggregated with ammonium sulfate and have round rims (Figure 7b). The

Si-Al-rich and organic particles are more abundant at the lower altitudes.

### 3.4. LS Out-of-Cloud Samples

[34] The number of particles on these grids is much smaller than in the UT samples.  $\text{H}_2\text{SO}_4$  droplets and ammonium sulfate particles comprise more than 90% of all particles (Table 2 and Figure 6). The  $\text{H}_2\text{SO}_4$  droplets are less ammoniated than those in the UT samples (Figure 2). EDS analysis revealed that many relatively large  $\text{H}_2\text{SO}_4$  droplets contain elements such as K, Fe, Si, Al, and Zn (Figure 8). These elements are probably from tiny inclusions in the  $\text{H}_2\text{SO}_4$  droplets (Figures 3c and 8a). Tiny ammonium sulfate particles are abundant, and large sulfate particles like those at the impaction center in the UT out-of-cloud samples (Figure 7a) are absent. Organic and Si-Al-rich particles also occur but are less abundant and smaller than in the UT samples (Table 2 and Figure 6).

## 4. Discussion

### 4.1. Characteristics of Major Solid Particles From the UT and LS

[35] Our organic particles (Figures 1b and 7b) contain a significant amount of K, suggesting a relationship to biomass burning. Recent TEM studies of particles from biomass burning in Africa report abundant occurrence of tar-like organic materials coexisting with KCl or  $\text{K}_2\text{SO}_4$  [*Li et al.*, 2003b; *Pósfai et al.*, 2003, 2004]. The organic particles in our samples might have originated from such mixtures. The particle analysis by laser mass spectrometry (PALMS), which was on the same WB-57F aircraft during the CRYSTAL-FACE mission, found many particles composed of sulfate species,  $\text{K}^+$ , organic fragments, and  $\text{NO}^+$  (abbreviated SKON) both inside and outside clouds [*Cziczko et al.*, 2004]. We believe our organic particles correspond to the SKON. Occurrence of rims around the organic particles (Figures 1b and 7b) suggests that these particles are hygroscopic.

[36] PALMS also detected signals from refractory species such as Al, Si, Fe, Mg, Ca, K, and Na, especially from ice residues during the 28 and 29 July flights when enhanced transport of Saharan dust was observed [*Cziczko et al.*, 2004]. We found only minor amounts of clay particles in samples from these dates. Most airborne clay particles, which are efficient IN [e.g., *Pruppacher and Klett*, 1997; *Zuberi et al.*, 2002], were plausibly incorporated in ice. CAPS data indicate that ice cloud particles were generally larger than several tens of micrometers across, too large to be collected by MACS.

[37] Particles rich in Si and Al are abundant (Figure 1c), and many differ in crystal structure and composition from common soil particles in the boundary layer. We obtained a chip of paint from the WB-57F aircraft and found that the paint contains significant amounts of Si and Al. Particles scraped from the paint chip show SAED patterns similar to those from the Si-Al-rich particles. Thus it is possible that some of the Si-Al-rich particles were derived from aircraft paints. They are particularly abundant in the LT sample (WB0726#23) and appear to have originated in the LT. Their poorly crystalline nature and sulfate coatings suggest that these Si-Al-rich particles are less efficient IN than clay particles.

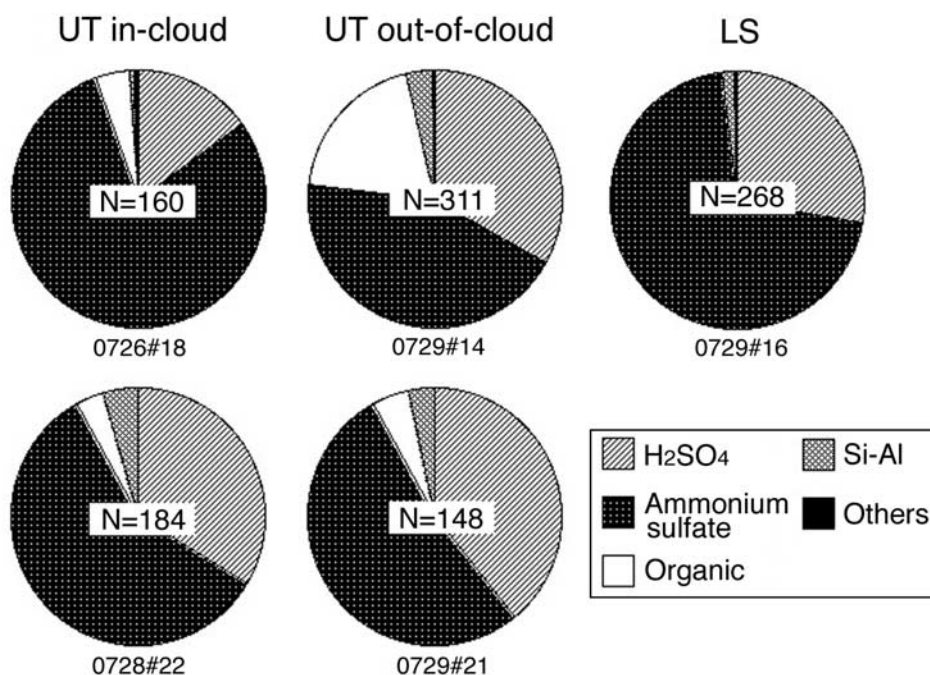


**Figure 6.** Proportions of UT in-cloud (0726#18 and 0728#22), UT out-of cloud (0729#14 and 0729#21), and LS (0729#16) aerosol samples. The number of analyzed particles is shown in each pie chart. Zn-rich particles are not included in the pie charts. The abundances of organic and Si-Al-rich particles decrease with altitude.

[38] The occurrence of Zn-rich particles (Figures 1d and 5) is puzzling. The amounts of Zn-rich particles correlate with those of ice particles detected during the sampling periods (Tables 1 and 2), suggesting a strong relationship between the Zn-rich and ice cloud particles. However, PALMS detected no Zn while flying in ice clouds [Murphy *et al.*, 2004]. Instead, it detected a lot of particles of stainless steel. Murphy *et al.* [2004] suggest that the stainless steel resulted from abrasion of the inner wall of the inlet by large ice crystals. We infer that Zn-rich particles in our samples are instrumental artifacts generated through a similar process. Their exact origin is currently unknown since an inspection of the sampling system did not reveal an obvious source.

#### 4.2. H<sub>2</sub>SO<sub>4</sub> Droplets in Tropical UT and LS

[39] A large fraction of the aerosol particles in the UT and LS are H<sub>2</sub>SO<sub>4</sub> droplets and other sulfate particles (Table 2 and Figure 6). Our MACS collected both interstitial and ice cloud particles, and we cannot distinguish between them. It is possible that the sulfate particles were mostly interstitial at the time of collection. However, these particles may freeze as temperature and RH change.

[40] H<sub>2</sub>SO<sub>4</sub> droplets on all analyzed grids contain central particles (Figures 1a and 3), suggesting that they were partially ammoniated prior to collection. Ammoniation of aerosols in the UT is of particular interest for ice cloud formation. Several experiments suggest that ammonium sulfate and bisulfate solutions exhibit less supercooling than H<sub>2</sub>SO<sub>4</sub> [Chen *et al.*, 2000; Chelf and Martin, 2001; Cziczo and Abbatt, 2001; Prenni *et al.*, 2001], although Koop *et al.* [2000] propose that the supercooling depends only on water activity and is independent of solute. The discrepancy may result from different experimental techniques. Ammoniation of H<sub>2</sub>SO<sub>4</sub> droplets possibly alters ice nucleation from

homogeneous to heterogeneous and thus facilitates freezing [Martin, 1998; Tabazadeh and Toon, 1998].

[41] Our TEM observations also show evidence that internal mixing of H<sub>2</sub>SO<sub>4</sub> with both soluble and insoluble materials is common in the UT and LS. Many H<sub>2</sub>SO<sub>4</sub> droplets leave C- and S-rich residues upon exposure to the electron beam (Figure 3), suggesting that they contain organic materials. Some also contain sulfates of metals such as Mg, Ca, K, and Fe. Small particles of organic and metal-rich materials and soot are common in H<sub>2</sub>SO<sub>4</sub> droplets (Figures 3c and 8a). Previous PALMS studies [Murphy *et al.*, 1998; Cziczo *et al.*, 2001] reported that stratospheric particles contain Fe, Mg, Na, Al, K, Ca, Cr, and Ni that are probably from meteoritic materials. Interplanetary dust particles (IDPs) collected in the stratosphere consist mainly of silicates, oxides, sulfides, and metal [Brownlee, 1985]. The tiny metal-rich inclusions in H<sub>2</sub>SO<sub>4</sub> droplets (Figures 3c and 8b) may correspond to such insoluble meteoritic materials. These inclusions can act as heterogeneous nuclei and promote ice formation.

[42] Some IDPs also contain carbonates that are soluble in H<sub>2</sub>SO<sub>4</sub> [Brownlee, 1985; Tomeoka and Buseck, 1986]. Mixing of H<sub>2</sub>SO<sub>4</sub> with soluble metal may also have significant effects on ice formation. Recent experiments on freezing of H<sub>2</sub>SO<sub>4</sub> containing soluble Fe and meteoritic metal show that a large part of the metal-containing H<sub>2</sub>SO<sub>4</sub> froze approximately 12 to 20 K higher than solutions containing no soluble metal [Wise *et al.*, 2003].

#### 4.3. Comparison Among the UT In-Cloud, Out-of-Cloud, and LS Samples

[43] The most remarkable difference between aerosol particles in and out of clouds is the abundance of Zn-rich particles (Table 2). Another difference can be found in the

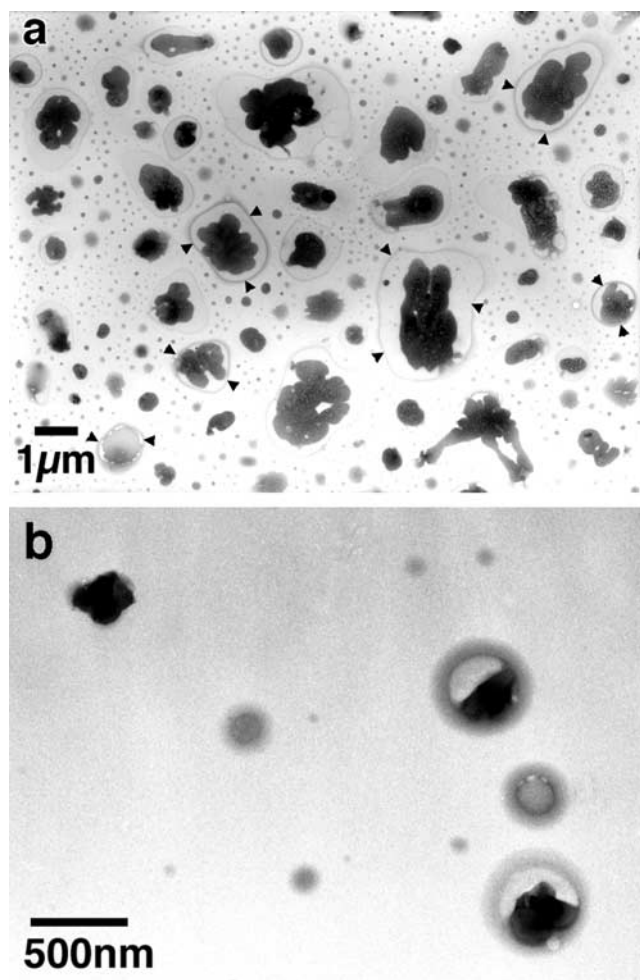


**Figure 7.** (a) Area at grid impactation center in a UT out-of-cloud sample. Many large sulfate particles occur that display rims (arrows). (b) Organic particles with (two on the right) and without (upper left) rims. They are aggregated with ammonium sulfate.

ratio of ammonium sulfate particles to  $\text{H}_2\text{SO}_4$  droplets (Figure 6). Round particles of Zn-sulfate are abundant in the in-cloud samples and are mixed with ammonium sulfate (Figure 5a), which is partly responsible for the higher ratio than for out-of-cloud samples. Also, they are larger than pure ammonium sulfate particles in out-of-cloud samples (Figure 4). They have close relationships to Zn-rich particles, i.e., correlated abundance and similar composition to coatings on Zn-rich particles, and thus are apparently related to ice cloud particles. It is possible that they contain materials from melted ice particles.

[44] Figure 2 shows that  $\text{H}_2\text{SO}_4$  droplets in cloud samples exhibit higher values of core/ring diameters than those in out-of-cloud samples, which indicates extensive ammoniation and suggests that more ammonia was available in clouds, perhaps from vertical transport from the LT by convection.

[45] Figure 2 also shows that  $\text{H}_2\text{SO}_4$  droplets in the LS are less ammoniated than those in the UT. *Sheridan et al.* [1994] studied aerosol particles from the UT and LS in midlatitudes and reported that  $\text{H}_2\text{SO}_4$  droplets from the LS

exhibit larger size distributions than those from the UT. The trend is also apparent in our samples (Figure 2). However, the satellite-ring diameter of a  $\text{H}_2\text{SO}_4$  droplet depends on both the original droplet size and its acidity [Bigg, 1975; Gras and Ayers, 1979]. From our current results, we cannot tell if  $\text{H}_2\text{SO}_4$  droplets in the LS before impactation were larger than those in the UT.

[46] UT out-of-cloud samples contain many large ( $>2 \mu\text{m}$ ) ammonium sulfate particles (Figure 7a). They have rims, which suggests that they originally contained a significant amount of water.  $\text{H}_2\text{SO}_4$ ,  $\text{NH}_4\text{HSO}_4$ , and  $(\text{NH}_4)_2\text{SO}_4$  are hygroscopic and form droplets at high RH [e.g., Pruppacher and Klett, 1997; Seinfeld and Pandis, 1998]. Such large, presumably aqueous sulfate particles are absent in the LS samples. The RH decreases steeply across the tropical tropopause [Vömel et al., 2002]. The dryness of the LS might have prevented sulfate particles from growing as large as in the UT.

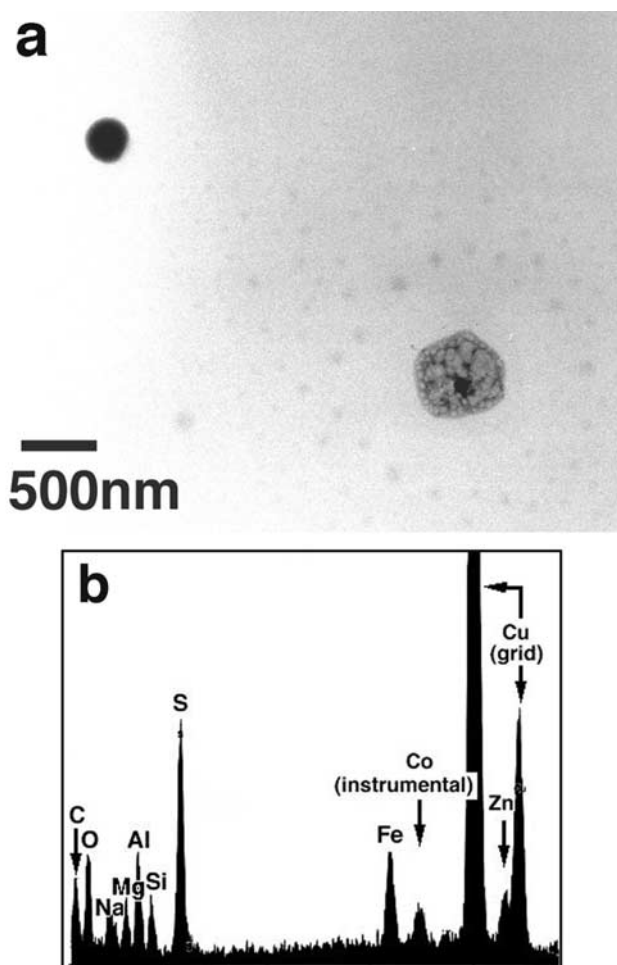


**Figure 8.** (a) A  $\text{H}_2\text{SO}_4$  droplet (lower right) and an ammonium sulfate particle (upper left) in a LS sample. The  $\text{H}_2\text{SO}_4$  droplet encloses a solid particle in its center. The sulfate particle has dark contrast. (b) EDS spectrum from the ammonium sulfate particle in Figure 8a. The spectrum indicates that the particle contains significant Fe, Zn, Al, Si, and Mg in addition to S and O. Elements other than S and O are probably from tiny inclusions mixed with sulfate.

[47] The proportion of organic and Si-Al-rich particles in all aerosol particles generally decreases with increasing altitude (Table 2 and Figure 6). There seems to be no significant difference between the UT in- and out-of-cloud samples regarding amounts of organic and Si-Al-rich particles. These nonsulfate particles also occur in the LS and are less abundant than in the UT. They were presumably transported upward from the troposphere and into the LS.

## 5. Conclusions

[48] Individual particle analysis by TEM provides detailed information regarding aerosol particles in the tropical UT and LS. The K-rich composition of organic particles in our samples, likely corresponding to the SKON detected by PALMS [Cziczo *et al.*, 2004], suggests that they are products of biomass burning. Significant enhancement of clay particles during a Saharan dust event was not observed in our UT and LS samples. This may be because they were preferentially incorporated into ice cloud particles that were too large to be collected by our sampling system. Abundant Zn-rich particles in in-cloud samples are probably artifacts that resulted from ice particles hitting inner parts of the sampling system.

[49] Sulfate particles dominate in all samples. The morphology of  $\text{H}_2\text{SO}_4$  droplets suggests that they were partially ammoniated prior to collection. In many  $\text{H}_2\text{SO}_4$  droplets,  $\text{H}_2\text{SO}_4$  was internally mixed with organic materials, soluble metal sulfates and chlorides, and insoluble solid particles. Because of the extensive ammoniation and internal mixing,  $\text{H}_2\text{SO}_4$  droplets from convective systems may promote heterogeneous ice nucleation.

[50] UT cloud samples were more ammoniated than UT out-of-cloud and LS samples, presumably because more ammonia was available as a result of convective transport from the LT. LS samples lack the relatively large aqueous sulfate particles that are common in UT out-of-cloud samples, indicating the dryness of the tropical LS compared to the UT. The proportion of nonsulfate particles to all aerosol particles decreases with increasing altitudes.

[51] **Acknowledgments.** We thank D. Murphy, D. Cziczo, S. Lee, J. Li, C. Twohy, P. DeMott, B. Toon, and A. Heymsfield for valuable information and discussion and D. Baumgardner, R. Herman, and E. Weinstock for sharing their data. We also thank S. Baccus and B. Gandrud for providing a paint sample from the WB-57F aircraft and information. This work was supported by NASA grant NAG5-11552. Work performed by M.J.M. was carried out at the Jet Propulsion Laboratory, California Institute of Technology, under a contract with the National Aeronautics and Space Administration.

## References

- Baumgardner, D., H. Jonsson, W. Dawson, D. O'Connor, and R. Newton (2001), The cloud, aerosol and precipitation spectrometer: A new instrument for cloud investigations, *Atmos. Res.*, 59–60, 251–264.
- Bigg, E. K. (1975), Stratospheric particles, *J. Atmos. Sci.*, 32, 910–917.
- Bigg, E. K. (1980), Comparison of aerosol at four baseline atmospheric monitoring stations, *J. Appl. Meteorol.*, 19, 521–533.
- Bigg, E. K., A. Ono, and W. J. Thompson (1970), Aerosols at altitudes between 20 and 37 km, *Tellus*, 22, 550–563.
- Brownlee, D. E. (1985), Cosmic dust: Collection and research, *Annu. Rev. Earth Planet. Sci.*, 13, 147–173.
- Buseck, P. R., and M. Pósfai (1999), Airborne minerals and related aerosol particles: Effects on climate and the environment, *Proc. Natl. Acad. Sci. U. S. A.*, 96, 3372–3379.
- Chelf, J. H., and S. T. Martin (2001), Homogeneous ice nucleation in aqueous ammonium sulfate aerosol particles, *J. Geophys. Res.*, 106, 1215–1226.
- Chen, Y., S. M. Kreidenweis, L. M. McInnes, D. C. Rogers, and P. J. DeMott (1998), Single particle analyses of ice nucleating aerosols in the upper troposphere and lower stratosphere, *Geophys. Res. Lett.*, 25, 1391–1394.
- Chen, Y., P. J. DeMott, S. M. Kreidenweis, D. C. Rogers, and D. E. Sherman (2000), Ice formation in sulfate and sulfuric acid aerosol particles under upper tropospheric conditions, *J. Atmos. Sci.*, 37, 3751–3766.
- Cziczo, D. J., and J. P. D. Abbatt (2001), Ice nucleation in  $\text{NH}_4\text{HSO}_4$ ,  $\text{NH}_4\text{NO}_3$ , and  $\text{H}_2\text{SO}_4$  aqueous particles: Implications for cirrus cloud formation, *Geophys. Res. Lett.*, 28, 963–966.
- Cziczo, D. J., D. S. Thomson, and D. M. Murphy (2001), Ablation, flux, and atmospheric implications of meteors inferred from stratospheric aerosol, *Science*, 291, 1772–1775.
- Cziczo, D. J., D. M. Murphy, P. K. Hudson, and D. S. Thomson (2004), Single particle measurements of the chemical composition of cirrus ice residue during CRYSTAL-FACE, *J. Geophys. Res.*, 109, D04201, doi:10.1029/2003JD004032.
- Denning, R. F., S. L. Guidero, G. S. Parks, and B. L. Gary (1989), Instrument description of the airborne microwave temperature profiler, *J. Geophys. Res.*, 94, 16,757–16,765.
- Ferek, R. J., A. L. Lazrus, and J. W. Winchester (1983), Electron microscopy of acidic aerosols collected over the northeastern United States, *Atmos. Environ.*, 17, 1545–1561.
- Gras, J. L., and G. P. Ayers (1979), On sizing impacted sulfuric acid aerosol particles, *J. Appl. Meteorol.*, 18, 634–638.
- Isono, K. (1955), On ice-crystal nuclei and other substances found in snow crystals, *J. Meteorol.*, 12, 456–461.
- Isono, K., M. Kobayashi, T. Takeda, T. Tanaka, K. Iwai, and M. Fujiwara (1971), Concentration and nature of ice nuclei in rim of the North Pacific Ocean, *Tellus*, 23, 40–59.
- Jonsson, H. H., *et al.* (1995), Performance of a focused cavity aerosol spectrometer for measurements in the stratosphere of particle size in the 0.06–2.0 micrometer diameter range, *J. Oceanic Atmos. Technol.*, 12, 115–129.
- Katrinak, K. A., P. Rez, and P. R. Buseck (1992), Structural variations in individual carbonaceous particles from an urban aerosol, *Environ. Sci. Technol.*, 26, 1967–1976.
- Koop, T., B. Luo, A. Tsias, and T. Peter (2000), Water activity as the determinant for homogeneous ice nucleation in aqueous solutions, *Nature*, 406, 611–614.
- Kumai, M. (1961), Snow crystals and the identification of nuclei in the northern U.S.A., *J. Meteorol.*, 18, 139–150.
- Kumai, M. (1976), Identification of nuclei and concentrations of chemical species in snow crystals sampled at the South Pole, *J. Atmos. Sci.*, 33, 833–841.
- Levin, Z., C. Price, and E. Ganor (1990), The contribution of sulfate and desert aerosols to the acidification of clouds and rain in Israel, *Atmos. Environ., Part A*, 24, 1143–1151.
- Li, J., J. R. Anderson, and P. R. Buseck (2003a), TEM study of aerosol particles from clean and polluted marine boundary layers over the North Atlantic, *J. Geophys. Res.*, 108(D6), 4189, doi:10.1029/2002JD002106.
- Li, J., M. Pósfai, P. V. Hobbs, and P. R. Buseck (2003b), Individual aerosol particles from biomass burning in southern Africa: 2. Compositions and aging of inorganic particles, *J. Geophys. Res.*, 108(D13), 4848, doi:10.1029/2002JD002310.
- Martin, S. (1998), Phase transformation of the ternary system  $(\text{NH}_4)_2\text{SO}_4$ – $\text{H}_2\text{SO}_4$ – $\text{H}_2\text{O}$  and the implication for cirrus cloud formation, *Geophys. Res. Lett.*, 25, 1657–1660.
- May, R. D. (1998), Open-path, near-infrared tunable diode laser spectrometer for atmospheric measurements of  $\text{H}_2\text{O}$ , *J. Geophys. Res.*, 103, 19,161–19,172.
- Murphy, D. M., D. S. Thomson, and M. J. Mahoney (1998), In situ measurements of organics, meteoritic material, mercury, and other elements in aerosols at 5 to 19 kilometers, *Science*, 282, 1664–1669.
- Murphy, D. M., D. J. Cziczo, P. K. Hudson, D. S. Thomson, J. C. Wilson, T. Kojima, and P. R. Buseck (2004), Particle generation and resuspension in aircraft inlets when flying in clouds, *Aerosol Sci. Technol.*, 38(4), 400–408.
- Popovitcheva, O. B., N. M. Persiantseva, M. E. Trukhin, G. B. Rulev, N. K. Shonija, Y. Y. Buriko, A. M. Starik, B. Demirdjian, D. Ferry, and J. Suzanne (2000), Experimental characterization of aircraft combustion soot: Microstructure, surface area, porosity and water adsorption, *Phys. Chem. Chem. Phys.*, 2, 4421–4426.
- Pósfai, M., and A. Molnár (2000), Aerosol particles in the troposphere: A mineralogical introduction, in *Environmental Mineralogy, EMU Notes in Mineral.*, vol. 2, edited by D. J. Vaughan and R. Wogelius, pp. 197–252, Eötvös Univ. Press, Budapest.

- Pósfai, M., J. R. Anderson, P. R. Buseck, and H. Sievering (1999), Soot and sulfate aerosol particles in the remote marine troposphere, *J. Geophys. Res.*, **104**, 21,685–21,693.
- Pósfai, M., R. Simonics, J. Li, P. V. Hobbs, and P. R. Buseck (2003), Individual aerosol particles from biomass burning in southern Africa: 1. Compositions and size distributions of carbonaceous particles, *J. Geophys. Res.*, **108**(D13), 8483, doi:10.1029/2002JD002291.
- Pósfai, M., A. Gelencsér, R. Simonics, K. Arató, J. Li, P. V. Hobbs, and P. R. Buseck (2004), Atmospheric tar balls: Particles from biomass and biofuel burning, *J. Geophys. Res.*, **109**, D06213, doi:10.1029/2003JD004169.
- Prenni, A. J., M. E. Wise, S. D. Brooks, and M. A. Tolbert (2001), Ice nucleation in sulfuric acid and ammonium sulfate particles, *J. Geophys. Res.*, **106**, 3037–3044.
- Pruppacher, H. R., and J. D. Klett (1997), *Microphysics of Clouds and Precipitation*, Kluwer Acad., Norwell, Mass.
- Seinfeld, J. H., and S. N. Pandis (1998), *Atmospheric Chemistry and Physics*, John Wiley, Hoboken, N. J.
- Sheridan, P. J., C. A. Brock, and J. C. Wilson (1994), Aerosol particles in the upper troposphere and lower stratosphere: Elemental composition and morphology of individual particles in northern midlatitudes, *Geophys. Res. Lett.*, **21**, 2587–2590.
- Tabazadeh, A., and O. B. Toon (1998), The role of ammoniated aerosols in cirrus cloud formation, *Geophys. Res. Lett.*, **25**, 1379–1382.
- Tomeoka, K., and P. R. Buseck (1986), A carbonate-rich, hydrated, interplanetary dust particle: Possible residue from protostellar clouds, *Science*, **231**, 1544–1546.
- Twohy, C. H., and B. W. Gandrud (1998), Electron microscope analysis of residual particles from aircraft contrails, *Geophys. Res. Lett.*, **25**, 1359–1362.
- Vömel, H., et al. (2002), Balloon-borne observations of water vapor and ozone in the tropical upper troposphere and lower stratosphere, *J. Geophys. Res.*, **107**(D14), 4210, doi:10.1029/2001JD000707.
- Weinstock, E. M., E. J. Hintsa, A. E. Dessler, J. F. Oliver, N. L. Hazen, J. N. Demusz, N. T. Allen, L. B. Lapon, and J. G. Anderson (1994), New fast response photofragment fluorescence hygrometer for use on the NASA ER-2 and the Perseus remotely piloted aircraft, *Rev. Sci. Instrum.*, **65**, 3544–3554.
- Wise, M. E., S. D. Brooks, R. M. Garland, D. J. Cziczo, S. T. Martin, and M. A. Tolbert (2003), Solubility and freezing effects of  $\text{Fe}^{2+}$  and  $\text{Mg}^{2+}$  in  $\text{H}_2\text{SO}_4$  solutions representative of upper tropospheric and lower stratospheric sulfate particles, *J. Geophys. Res.*, **108**(D14), 4434, doi:10.1029/2003JD003420.
- Zuberi, B., A. K. Bertram, C. A. Cassa, L. T. Molina, and M. J. Molina (2002), Heterogeneous nucleation of ice in  $(\text{NH}_4)_2\text{SO}_4$ – $\text{H}_2\text{O}$  particles with mineral dust immersions, *Geophys. Res. Lett.*, **29**(10), 1504, doi:10.1029/2001GL014289.

P. R. Buseck, Department of Geological Sciences, Arizona State University, Tempe, AZ 85287, USA. (pbuseck@asu.edu)

T. Kojima, Faculty of Science, Kumamoto University, Kumamoto 860-8555, Japan. (tkojima@sci.kumamoto-u.ac.jp)

M. J. Mahoney, Jet Propulsion Laboratory, California Institute of Technology, MS 246-101, 4800 Oak Grove Drive, Pasadena, CA 91109-8099, USA. (michael.j.mahoney@jpl.nasa.gov)

J. M. Reeves and J. C. Wilson, Department of Engineering, University of Denver, 2390 S. York Street, Denver, CO 80208, USA. (jreeves@du.edu; jwilson@du.edu)